energy&fuels

pubs.acs.org/EF

Article

Stabilization and Emission Characteristics of Gliding Arc-Assisted NH_3/CH_4/Air Premixed Flames in a Swirl Combustor

Jinguo Sun, Qian Huang, Yong Tang, and Shuiqing Li*

Cite This: *Energy Fuels* 2022, 36, 8520−8527

Read Online

ACCESS | Metrics & More | Article Recommendations | Supporting Information

ABSTRACT: This paper investigates the effects of gliding arc (GA) discharge on the stabilization and emission characteristics of premixed NH_3/CH_4/air swirl flames under various ammonia contents, flow rates, and global equivalence ratios. First, the lean blowout (LBO) limits are measured. We find that although blending CH_4 extends the LBO limit of the ammonia flame to 0.6−0.8, the GA discharge further remarkably extends it to 0.3−0.4. Then, the flow and flame structures are visualized by simultaneous OH planar laser-induced fluorescence and particle imaging velocimetry measurements. The results reveal that the discharge increases the OH radical concentration and expands the inner recirculation zone, leading to improved flame stability. Second, the NO_x emissions are investigated over a wide range of global equivalence ratios and ammonia contents. It is seen that the GA discharge slightly increases the NO_x emission by less than 7% at low NH_3 contents (<0.6), which can be attributed to the thermal and OH-involved reaction pathway of NO_x formation. However, as the NH_3 content further increases (which is accompanied by the rapid growth of the NO_x emission), the GA discharge effectively reduces the NO_x emission by up to 30%. This effect might be due to the more intensive NO_x-consuming reactions by plasma-induced NH_2 radicals at a higher ammonia content, which is confirmed by the strengthened NH_2* chemiluminescence under GA discharge conditions. Finally, a chemical reactor network analysis gives reasonable NO_x predictions without GA discharge and highlights the NO_x-reduction effects of NH_2 radicals under high ammonia contents.

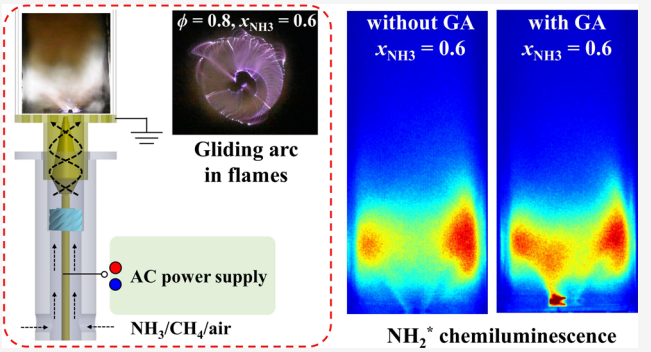

1. INTRODUCTION

Concerns for global climate change have led to a rekindled interest in ammonia (NH_3) as a promising carbon-free fuel for local energy storage at scale and sustainable transportation.[1−4] Ammonia, as a superior energy carrier, has an energy density of 18.8 MJ/kg, outperforming almost all other potential hydrogen carriers. The mature infrastructure network of ammonia production, storage, and utilization further enhances its commercial viability. All of these make ammonia the most suitable for large-capacity power generation, with few technology and safety barriers.[5,6] However, the clean and efficient combustion of ammonia remains challenging due to its narrow flammability ranges and the high propensity to form nitric oxides (NO_x),[3] which limits the operational envelope and thermodynamic performance of gas turbines.[5]

To tackle this issue, combustion technologies are projected to progress over time from conventional fossil fuels to blends of ammonia and hydrocarbon fuels.[7] It has been revealed that co-firing ammonia with H_2,[8−12] CH_4,[13−17] and diesel[18] enjoys not just reduced CO_2 emissions but also improved combustion and thermal efficiencies. Compared with pure ammonia, premixed NH_3/CH_4 flames have enhanced laminar flame speeds and extended lean blowout (LBO) limits,[19,20] whereas the extended LBO limits (from 0.63 to 0.48) are far from satisfactory. Besides, the NO_x problem of co-firing NH_3/CH_4 flames grows even worse than that of pure ammonia.[20,21] For example, when the molar fraction of NH_3 is 50%, the NO concentration can reach ∼6 times that of a pure ammonia flame.[20,21] Therefore, researchers are struggling to seek a novel strategy for the better performance of burning NH_3/CH_4 blends for potential use in power generation.

Plasma-assisted combustion (PAC) is a proactive control technology for ignition and flame stabilization, and the past few decades have seen its application in aircraft engines.[22,23] It is hence appealing to explore the potential benefits of plasma for ammonia-fueled flames. Several recent studies show positive effects of plasma on laminar flame speed and ignition delays of pure ammonia combustion,[24,25] focusing on the plasma-assisted kinetic models. Choe et al. preliminarily examined the effects of plasma on the LBO and NO_x emission

Received: April 19, 2022
Revised: July 6, 2022
Published: July 14, 2022

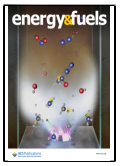

https://doi.org/10.1021/acs.energyfuels.2c01217
Energy Fuels 2022, 36, 8520−8527

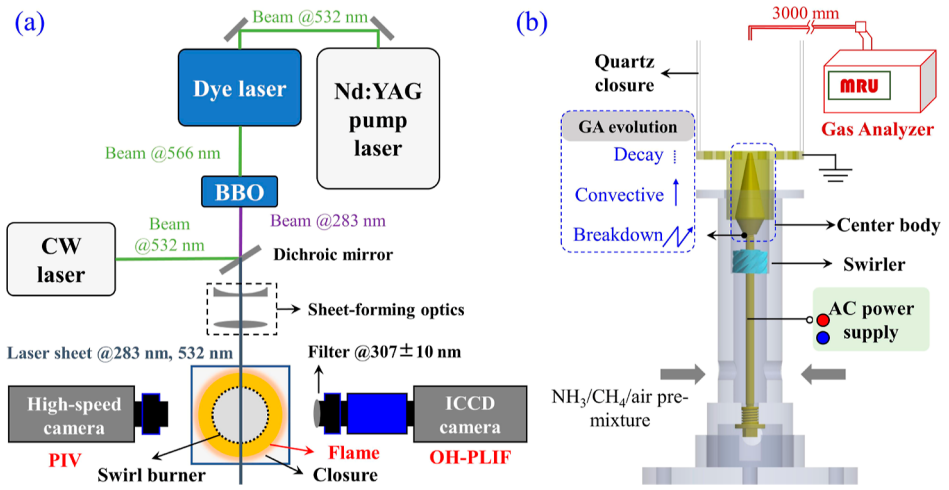

Figure 1. Schematic of the experimental setup including (a) simultaneous PLIF/PIV system and (b) premixed swirl burner integrated with the GA discharge and the exhaust gas sampling system.

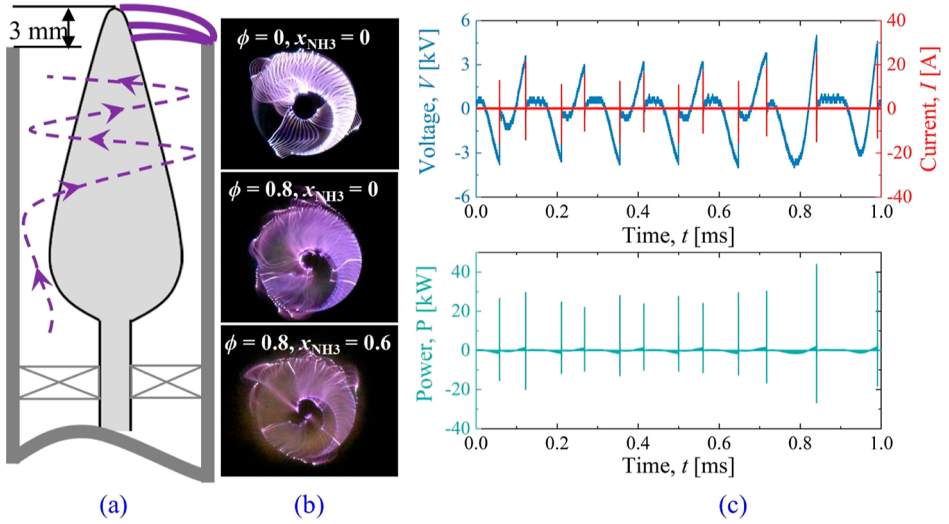

Figure 2. (a) Schematic of GA evolution, (b) emissions of the GA discharge sustained in air and the NH_3/CH_4/air flame, and (c) voltage and current waveforms of the GA discharge.

of ammonia flames. They found that the nanosecond pulsed discharge can reduce NO_x emission and extend the LBO limits of ammonia flames.[26] However, the underlying mechanism of the plasma-assisted flame stabilization and related emission characteristics remains largely unknown.

Among various plasmas including microwave discharges,[27,28] radio frequency discharges,[29] nanosecond/microsecond repetitively pulsed discharges,[30−33] and gliding arc (GA) discharges,[34−37] we choose the GA discharge as the plasma actuator. As an ideal intermediate between thermal and nonthermal plasmas, the GA discharge possesses not only a relatively high plasma density but also high electron temperature and chemical selectivity.[38] We have found that the GA discharge significantly extended the LBO limits of methane flames.[39,40] More recently, it was used to stabilize pure ammonia flames.[41,42] Aiming at the future practical use of PAC for NH_3/CH_4 mixtures, the GA performance on the premixed swirl flames (PSFs), which is an important feature in modern combustors, needs to be thoroughly illustrated.

In this paper, we investigate the effects of GA discharge on the LBO limits and NO_x emissions of well-developed NH_3/CH_4/air PSFs. Operating parameters including the ammonia fraction, the global equivalence ratio, and the flow rates are manipulated. Optical diagnostic techniques, including simultaneous OH planar laser-induced fluorescence and particle imaging velocimetry (OH-PLIF/PIV) and NH_2* chemiluminescence, are utilized to give insights into the plasma-assisted flame structure and emissions. Finally, the chemical reactor network (CRN) analysis based on the CHEMKIN platform[43] is performed to model the premixed swirl combustion with NH_3/CH_4/air chemistry, which further identifies the role of GA in modifying ammonia reaction pathways.

2. EXPERIMENTAL SETUP

2.1. Premixed Swirl Burner and the GA Discharge System.

Figure 1 shows a schematic of the experimental setup, including the premixed swirl burner integrated with a GA discharge configuration and a simultaneous OH-PLIF/PIV system. The burner consists of an injector with an inner diameter (d_i) of 20 mm, a conical center body of 8 mm diameter (d_c) tapering to 2 mm diameter, an eight-blade swirler with a blade inclination angle of $\alpha = 45°$, and a 70 × 70 × 200 mm^3 square quartz closure. The gas mixture of NH_3/CH_4/air flows

https://doi.org/10.1021/acs.energyfuels.2c01217
Energy Fuels 2022, 36, 8520−8527

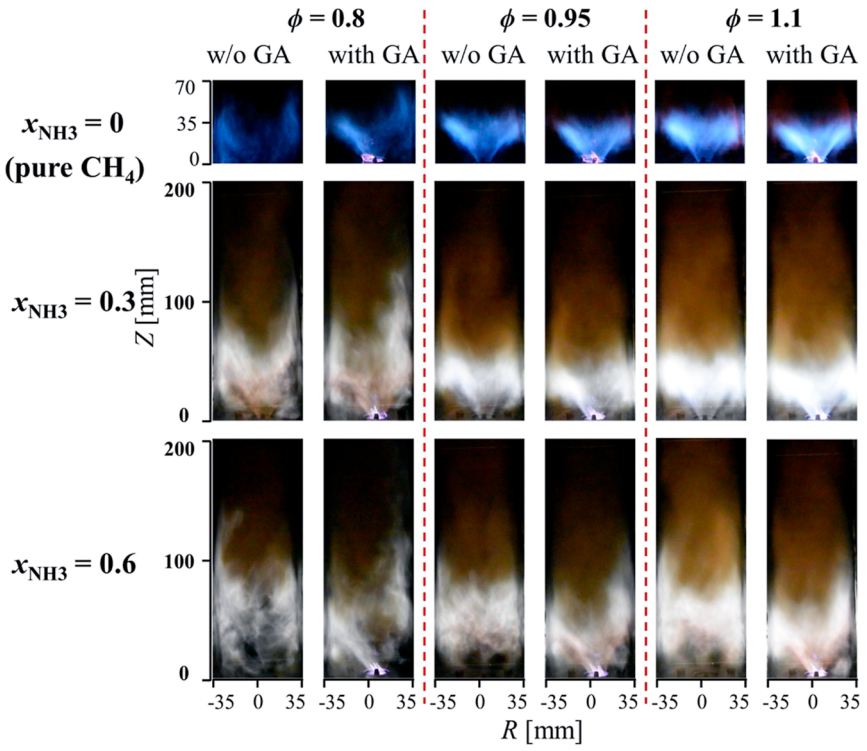

Figure 3. Direct photography of NH_3/CH_4/air flames at various equivalence ratios and NH_3 fuel ratios, without and with GA discharges.

through the swirler to produce a swirling flow with a swirl number (Sw) of 0.75, which is calculated from the formula[44]

$$\mathrm{Sw} = \frac{2}{3}\tan(\alpha)\frac{1-(d_c/d_i)^3}{1-(d_c/d_i)^2} \quad (1)$$

It should be noted that compared with the conventional cylindrical center body, the conical center body does not change the extinction limits in the current examinations.

The continuous rotational GA discharge is effectively generated through the following circuit configuration: the center body is connected to an alternating current power supply to serve as the high-voltage electrode, while the outer nozzle is grounded. A quartz plate is placed on the nozzle outlet as an insulator. The arc initially forms at the narrowest gap (~1 mm) between two diverging electrodes ("breakdown") and then propagates upward with the gas flow ("convection") and eventually decays ("decay"), constituting the periodic evolution of the GA discharge (see Figure 2a).[38] Figure 2b shows top-view visualizations of the GA discharges sustained in NH_3/CH_4/air flows with different ammonia contents, recorded using a CMOS digital camera (Nikon D5600). We measure the voltage and current waveforms of the discharge using a high-voltage probe (Tektronix P6015A, 4 ns rise time) and a current probe (Pearson 4100, 10 ns rise time), respectively, and record the waveforms using an oscilloscope (Tektronix DPO2024B, 1 GS/s sample rate), as shown in Figure 2c. For the rotational GA discharge, the discharge frequency is ~7 kHz, and the energy deposition is ~200 W, which is smaller than 1% of the combustion power of 3 kW, assuming a complete fuel consumption.

2.2. Simultaneous OH-PLIF/PIV Measurement and NH_2* Chemiluminescence. As illustrated in Figure 1, a dichroic mirror prior to the sheet-forming optics is used to spatially overlap the 283 nm beam from a dye laser (Cobra-Stretch) operated at 5 Hz for OH-PLIF and the 532 nm beam from a continuous-wave laser (MGL-W, 18 W) for PIV, allowing the simultaneous OH-PLIF/PIV measurements. The detailed descriptions are available in our previous work.[40] OH-PLIF images are captured using an intensified charge-coupled device (ICCD, PIMAX-IV, 1024 × 1024 pixels) camera equipped with a 307 ± 10 nm filter and PIV images using a high-speed camera (Phantom v311, 1024 × 1024 pixels) at a frame rate of 4200 fps and an exposure time of 50 μs. The feasibility of PIV measurements in the weakly ionized flow was previously demonstrated.[45] PLIF and PIV cameras are triggered synchronously using a digital delay generator (Stanford Research Systems, model DG645, <25 ps rms jitter).

NH_2* chemiluminescence is measured to reveal the intermediate chemistry of NH_3/CH_4 combustion. The direct proportionality between the electronically excited (NH_2*) and ground states (NH_2) justifies the use of the intensity of NH_2* chemiluminescence to represent the population of ground state NH_2.[46] A single peak of the NH_2-α band is featured using a 632.8 ± 3 nm filter,[47] and the emissions are collected using the ICCD camera with a gate width of 2 ms.

3. RESULTS AND DISCUSSION

3.1. Visual Observations of NH_3/CH_4/Air Flames. We test the NH_3/CH_4/air flames at various equivalence ratios (ϕ) and NH_3 fuel ratios (x_{NH_3}). x_{NH_3} is the mole fraction of NH_3 in the binary fuel of NH_3 and CH_4. Since N_2 rather than NO or NO_2 is considered the complete oxidation product of NH_3 combustion, the global reaction can be expressed as follows[19]

$$m\mathrm{CH_4} + n\mathrm{NH_3} + (2m + 0.75n)(\mathrm{O_2} + 3.76\mathrm{N_2}) \rightarrow m\mathrm{CO_2} + (2m + 1.5n)\mathrm{H_2O} + [3.76 \times (2m + 0.75n) + 0.5n]\mathrm{N_2} \quad (2)$$

The equivalence ratio is calculated as

$$\phi = \frac{[Q_{air}/(Q_{CH_4} + Q_{NH_3})]_{stoichiometric}}{Q_{air}/(Q_{CH_4} + Q_{NH_3})} \quad (3)$$

Figure 3 shows the typical images of NH_3/CH_4/air flames in the presence or absence of GA discharges. Different from the blue emission primarily from CH* chemiluminescence in the pure CH_4 flames ($x_{NH_3} = 0$), the NH_3/CH_4/air flames emit

https://doi.org/10.1021/acs.energyfuels.2c01217
Energy Fuels 2022, 36, 8520−8527

orange chemiluminescence, which is induced by the spectrums of the NH_2-α band and superheated water vapor.[48] In addition, compared to the ~35 mm height of CH_4/air flames, the NH_3 addition significantly increases the flame height due to the lower laminar burning velocity of premixed NH_3/CH_4/air flames (with the identical thermal input).[19]

In the absence of the GA, a continuous increase in x_{NH_3} at a fixed ϕ leads to a more unstable flame and weaker flame chemiluminescence. Taking the near-limit flame at $\phi = 0.8$ and $x_{NH_3} = 0.6$ as an example, the flame root can still be attached to the bluff body when the GA discharge is turned on. Meanwhile, the orange chemiluminescence appears to be strengthened, especially at the flame root that is directly processed by the arc. Since the orange emission mainly originates from the NH_2-α band, the modified orange chemiluminescence strongly suggests that the GA discharge not only affects the flame stability but also participates in the NH_3 decomposition.

3.3. Effectiveness of GA in Flame Stabilization. Figure 4 shows the LBO limits of NH_3/CH_4/air flames. We gradually reduce the fuel content in the pre-mixture until the flame extinction to obtain the extinction equivalence ratio (ϕ_{ext}). Each case is repeated at least three times to reduce randomness. The deviations of the repetitive measurements, together with the uncertainty of the flow meters (2%), are used to determine the uncertainties of the measurements. The flow rate varies from 20 to 100 L/min, and the Reynolds number ($Re = ud/\nu$) ranges from 1100 to 5800, assuming a constant kinematic viscosity (ν). It can be clearly seen that the blending of NH_3 narrows the LBO limit. Without (i.e., w/o) the discharge, as the x_{NH_3} increases from 0 to 0.6, ϕ_{ext} increases from ~0.60 to ~0.90, while on applying the GA discharge, the LBO limit can be extended from 0.66 to 0.93 to 0.29 to 0.53, indicating significant improvement (by 40−56%) of the flame stability. Moreover, even for high Reynolds numbers, GA discharges can still drastically extend the LBO limits, manifesting the potential effectiveness of the current GA for high-speed reacting flows. A comparison between dynamic evolutions of the PSFs without and with GA discharge can be found in the supplemental movie.

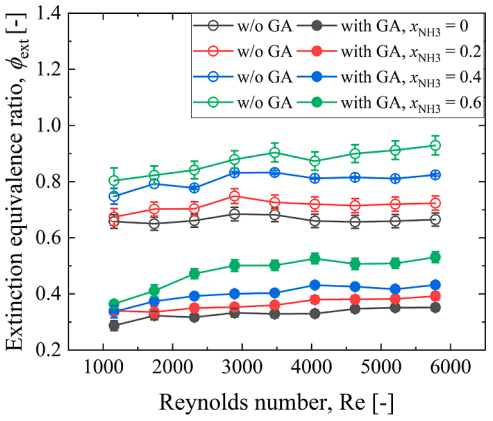

Figure 4. LBO limits of NH_3/CH_4/air flames without and with GA discharges.

When periodically rotating around the center body, the GA discharge processes the fresh reactant at a high frequency of ~7 kHz. It serves as a repetitive igniter to produce the flame kernel, which is critical to the flame reignition. The formation of the GA-induced flame kernel and its propagation were expatiated in our previous studies.[39] Consequently, the high-frequency repetitive ignition of the lean PSF contributes to a dramatic extension of the LBO limit.[39,40] Detailed effects of GA discharge on flame and flow structures are further exploited by optical measurements.

Figure 5 shows the time-averaged OH-PLIF/PIV images of PSFs without and with GA discharges, based on 200 snapshots. The OH contour superimposed by the velocity vectors identifies a typical confined V-shaped flame. It consists of a cone-shaped stream issuing from the nozzle outlet, an inner recirculation zone (IRZ) along the centerline, and an outer recirculation zone adjacent to the chamber walls. The OH-PLIF signal intensity decreases with x_{NH_3}, indicating a weakened burning intensity.[49] It results from the lower

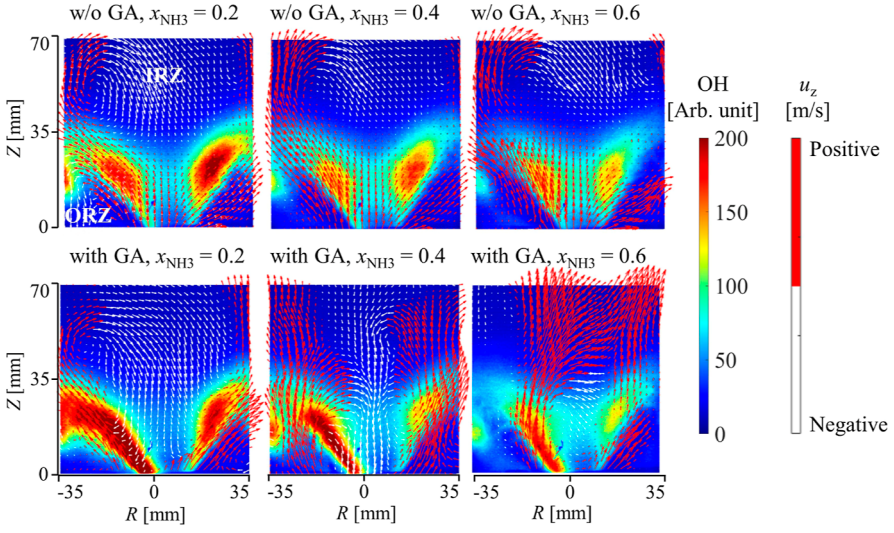

Figure 5. OH-PLIF images of PSFs without and with GA discharges ($\phi = 0.95$ and Re = 3500). Velocity vectors are superimposed on the OH-PLIF images, in which negative and positive axial velocities are displayed in white and red, respectively.

https://doi.org/10.1021/acs.energyfuels.2c01217
Energy Fuels 2022, 36, 8520−8527

reactivity of NH_3, which is consistent with the observation of the flame emissions.

At various ammonia contents, the GA discharge increases the OH signal intensity and expands the areas with high OH levels denoting the reaction zone. It should be noted that the PLIF image is not perfectly axisymmetric because there appear to be preferred locations for the arc. It was reported that the production of OH radicals and O atoms is accelerated by H atoms produced through electron collision: $NH_3 + e = NH_2 + H + e$.[25] The plasma-induced OH radical promotes ammonia decomposition via the chain propagation reaction: $NH_3 + OH = NH_2 + H_2O$, thus increasing the flame speed.[24] Conclusively, the population of the radical pool elevated by the GA discharge plays an important role in combustion chemistry and remarkably improves the stability of ammonia flames, as exploited by the LBO results. In addition, as demonstrated by the velocity vectors, although with a slight increase in asymmetry, the GA discharge results in a broadened IRZ, which ensures longer residence time for the fresh inflowing reactants to be burnt with the hot recirculated product and thus is more favorable for the flame stabilization. For instance, the estimated residence time is increased from ~16 to ~30 ms at $\phi = 0.95$ and $x_{NH_3} = 0.2$. The broadened IRZ and enhanced reaction zone were also observed in previous study on GA-assisted methane flames. The combustion enhancement can be attributed to a strong non-linear coupling between the plasma and the turbulent flame.[40] Apart from the effects on kinetics and the flow field, the thermal channel of GA was previously reported to have a less significant effect on the stabilization but a prominent effect on the ignition.[36] Conclusively, in terms of the LBO limit improvement, the GA in the current work might be regarded as an essentially high-repetition-rate igniter for the near-limit flame.

3.4. Effect of GA on NO_x Emissions. As shown in Figure 1b, we measured global NO_x emissions (including dominant NO and negligible NO_2) at the exhaust port using a gas analyzer (MRU 600). The flue gas was sampled using a probe placed at the exit plane of the quartz closure, 200 mm above the burner nozzle. The sampling probe with a very small cross-sectional area (~0.1% of that of the combustion chamber) caused negligible perturbations to the flames, which was verified by the tests with and without it. The sample line connected with the probe was heated at 393 K to eliminate the water condensation. The radial profile of NO_x emission was examined to verify the homogeneity of the exhaust gas. Meanwhile, the possible ammonia slip is monitored using another gas analyzer (RCP-M1). The results verify a complete consumption of NH_3 in our current configuration.

Figure 6 shows the NO_x emissions of NH_3/CH_4/air flames at different NH_3 fuel ratios and equivalence ratios. Note that the NO_x curve for $\phi = 0.7$ ranges within $x_{NH_3} = 0-0.3$ because a higher x_{NH_3} fails to stabilize the flame. Clearly, NO_x has a non-monotonic dependence on x_{NH_3}. In particular, the pure methane flame produces NO_x of ~50 ppmv, and the addition of NH_3 leads to a dramatic increase in NO_x in the order of 10^3 ppmv. With the increment of x_{NH_3}, NO_x emission peaks at ~50% for $\phi = 0.95/1.1$ and then decreases. Such decrement can be explained by the reaction with rich NH_3.[21] Moreover, for different equivalence ratios, the highest NO_x emission occurs at $\phi = 0.95$. This trend is compatible with measurements in refs 13 and 20, which was found to be similar to that of the OH-PLIF intensities.

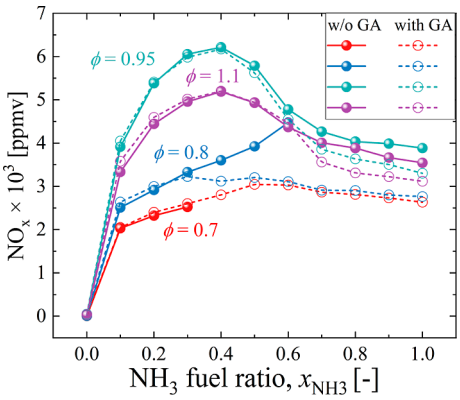

Figure 6. NO_x emissions of PSFs without and with GA discharges.

Furthermore, the effects of the GA on NO_x emissions are revealed in Figure 6. When x_{NH_3} is relatively small, the NO_x emissions are slightly increased when applying the GA. Such increment of NO_x emission may be attributed to the prominent thermal NO_x mechanism. In the non-equilibrium processes, more atomic N and O, which are generated by the electron impact dissociation reactions of N_2 and O_2, are supplied to form thermal NO via the reactions $N + O_2 = NO + O$ and $N_2 + O = NO + N$.[36] Besides, the plasma-induced OH radicals involved with the essential reaction of $N + OH = NO + H$ in the extended Zeldovich mechanism also contribute to NO production.[3]

At a higher level of x_{NH_3} (>0.3), the NO_x emission decreases with the presence of the GA. For $\phi = 1.1$ and $x_{NH_3} = 1.0$, the NO_x emission is decreased by ~20%. NO_x reduction was also found in previous work on pure ammonia flames assisted by nanosecond pulsed discharge.[26] The time-averaged NH_2* chemiluminescence associated with NO consumption was obtained from 200 snapshots.[47] We employ a three-point Abel-inversion method on the original (O) line-of-sight-integrated signals to transform them into the Abel-inverted (A) images,[50] as shown in the right half images of Figure 7. The non-equilibrium plasma was reported to provide another channel for NH_3 decomposition, that is, $NH_3 + e \rightarrow NH_2 + H + e$,[24,25] leading to the strengthened NH_2 chemiluminescence, as seen in Figure 7. It is a manifestation of enhanced ammonia combustion. Moreover, the increased NH_2 radical contributes to the NO consumption through the reaction $NH_2 + NO = N_2 + H_2O$ which is identified as the most important reaction in the thermal De-NO_x process.[51] To interpret the role of NH_2 in NO_x reduction, the reaction pathway of NO_x in the current configuration is addressed in section 3.5.

3.5. NO_x Reduction Mechanism. A chemistry reactor network (CRN) is further used to simulate mixing/flow characteristics of the swirl flame, which can drastically reduce the computational cost and still provide reasonable solutions.[52] Figure 8a shows a schematic of the hybrid CRN model consisting of two clusters. Cluster I consists of two perfectly stirred reactors (PSRs), representing the flame zone (PSR I) and the recirculation zone (PSR II), and cluster II uses a single plug flow reactor (PFR) to model the post-flame zone. Based on the simultaneous OH-PLIF/PIV measurement, the flame zone near the OH brush, the recirculation zone with reverse axial velocity components, and the post-flame zone with hot

https://doi.org/10.1021/acs.energyfuels.2c01217
Energy Fuels 2022, 36, 8520−8527

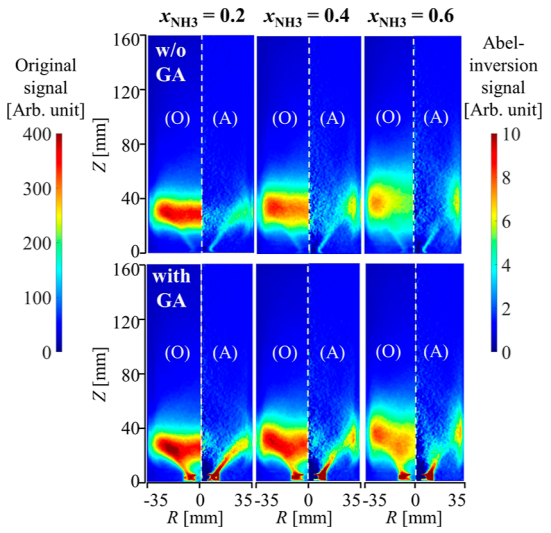

Figure 7. Original (O) and Abel-inverted (A) NH_2* chemiluminescence of PSFs without and with GA discharges (ϕ = 0.95 and Re = 3500).

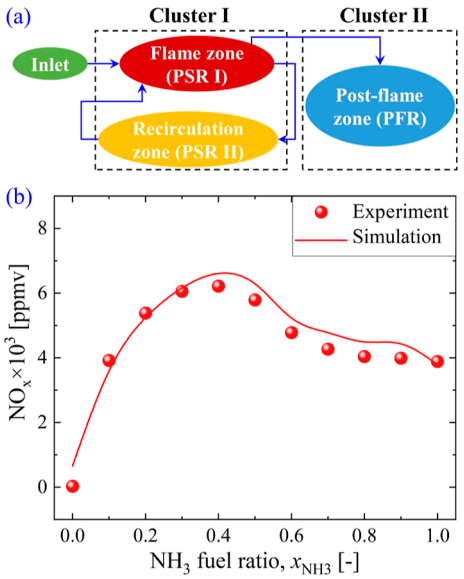

Figure 8. (a) Schematic of the CRN model configuration and (b) experimental and numerical results of flames at ϕ = 0.95 and Re = 3500.

products can be identified. The residence time for each reactor was estimated from the ratio of the size of the flame/recirculation zone to the average velocity. The recirculation between PSR I and PSR II is set to 20% of the product gases, and multiple iterations are required to achieve a convergent calculation. The inlet boundary conditions, including the temperature, flow rate, and mixture composition, are given according to the experimental operation. The CRN analysis employs an efficient and widely used chemical kinetic mechanism for NH_3/CH_4 combustion, which contains 42 species and 130 reactions.[19] A comparison between experimental and numerical results is shown in Figure 8b, with a maximum deviation smaller than 15% to validate the feasibility of the CRN analysis.

Figure 9 is the reaction pathway diagram at the flame zone, which is addressed on the flow of element N. Undergoing hydrogen abstraction, NH_3 molecules are converted to NH_x radicals, which then participate in the subsequent pathway: (i) oxidation leading to NO formation via the HNO intermediary or (ii) conversion to N_2.[51] Then, to figure out the influential reactions, the normalized NO sensitivity coefficient (SC) is defined as

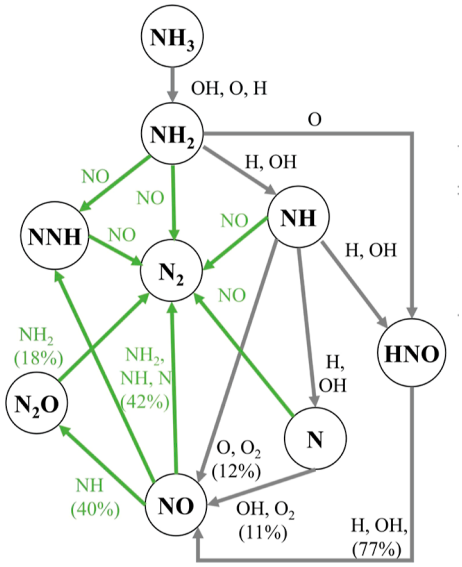

Figure 9. Reaction diagram for the N element.

$$SC = \frac{\partial \ln Y_{NO}}{\partial \ln k_i} \quad (4)$$

where Y_{NO} is the NO fraction and k_i is the reaction rate constant of the i-th reaction.[53]

Taking the case of ϕ = 0.95 as an example, the variations of the negative SC (−SC) of the top six influential reactions for NO consumption versus x_{NH_3} are plotted in Figure 10. These

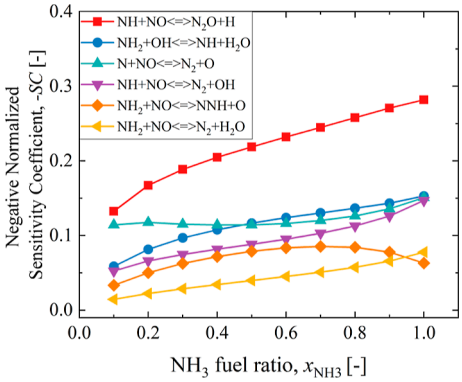

Figure 10. Dependence of sensitivity coefficient vs ammonia content.

reactions include (I) NH + NO ↔ N_2O +H, (II) NH_2 + OH ↔ NH +H_2O, (III) N + NO ↔ N_2 + OH, (IV) NH + NO ↔ N_2 + OH, (V) NH_2 + NO ↔ NNH + OH, and (VI) NH_2 + NO ↔ N_2 + H_2O. It suggests that the NO emission is dominated by the NH_x radicals. Moreover, the general increase in −SC versus x_{NH_3} pronounces the role of NH_x radicals in promoting NO consumption at a higher x_{NH_3}. Therefore, combined with the detected signals of NH_2* chemiluminescence, it can be concluded that the GA discharge facilitates the initial ammonia decomposition and produces more NH_x

https://doi.org/10.1021/acs.energyfuels.2c01217
Energy Fuels 2022, 36, 8520−8527

radicals, which are essential in the NO_x reduction at a higher ammonia content.

4. CONCLUSIONS

In this paper, we intensively investigate the stabilization and emission characteristics of the premixed NH_3/CH_4/air flame in GA discharges. First, it is revealed that the GA discharge can remarkably extend the LBO limits by up to 56% in a wide range of operation conditions (in terms of NH_3 fuel ratios, equivalence ratios, and flow rates). Apart from the high-frequency repetitive ignition provided by the GA discharge, the improved flame stabilities can be further attributed to the enhanced OH-rich reaction zone and the broadened IRZ under GA discharges.

Then, the GA exhibits complex influences on the NO_x emission of the NH_3/CH_4/air flames. At a low NH_3 content ($x_{NH_3} < 0.6$), the NO_x emission slightly increases with the presence of the GA discharge, which might be attributed to the enhanced thermal-NO_x pathway, whereas for $x_{NH_3} > 0.6$, the NO_x emission can be reduced by up to 30% after applying the GA discharge. Subsequently, through the CRN analysis for the premixed NH_3/CH_4/air swirl flame, we find that the NH_x radical plays an essential role in NO_x-consuming reactions. Besides, the NH_2* chemiluminescence measurements clearly show that the NH_2* signal intensity is significantly enhanced under GA discharge, that is, more NH_2 radicals can be produced. Therefore, the main reason for reduced NO_x emission under GA is the greater propensity of ammonia decomposition to NH_2 radicals under the bombardment of reactive electrons and radicals.

Future work on the integration of plasma dynamics with NH_3/CH_4 combustion chemistry is beneficial for the development of practical techniques, which is underway.

■ ASSOCIATED CONTENT

Supporting Information

The Supporting Information is available free of charge at https://pubs.acs.org/doi/10.1021/acs.energyfuels.2c01217.

Videos of NH_3/CH_4/air flames with and without GA (MP4)

■ AUTHOR INFORMATION

Corresponding Author

Shuiqing Li − *Key Laboratory for Thermal Science and Power Engineering of Ministry of Education, Department of Energy and Power Engineering, Tsinghua University, Beijing 100084, China;* orcid.org/0000-0001-6278-5956; Phone: +86-010-62788506; Email: lishuiqing@tsinghua.edu.cn; Fax: +86-010-62773384

Authors

Jinguo Sun − *Key Laboratory for Thermal Science and Power Engineering of Ministry of Education, Department of Energy and Power Engineering, Tsinghua University, Beijing 100084, China*

Qian Huang − *Key Laboratory for Thermal Science and Power Engineering of Ministry of Education, Department of Energy and Power Engineering, Tsinghua University, Beijing 100084, China*

Yong Tang − *School of Aerospace Engineering, Beijing Institute of Technology, Beijing 100081, China*

Complete contact information is available at: https://pubs.acs.org/10.1021/acs.energyfuels.2c01217

Notes

The authors declare no competing financial interest.

■ ACKNOWLEDGMENTS

This work is supported by the National Natural Science Foundation of China (grant nos. 51725601 and 91641204).

■ REFERENCES

(1) Valera-Medina, A.; Amer-Hatem, F.; Azad, A. K.; Dedoussi, I. C.; de Joannon, M.; Fernandes, R. X.; Glarborg, P.; Hashemi, H.; He, X.; Mashruk, S.; et al. Review on Ammonia as a Potential Fuel: From Synthesis to Economics. *Energy Fuels* **2021**, *35*, 6964−7029.

(2) Valera-Medina, A.; Xiao, H.; Owen-Jones, M.; David, W. I. F.; Bowen, P. J. Ammonia for power. *Prog. Energy Combust. Sci.* **2018**, *69*, 63−102.

(3) Kobayashi, H.; Hayakawa, A.; Somarathne, K. D. K. A.; Okafor, E. C. Science and technology of ammonia combustion. *Proc. Combust. Inst.* **2019**, *37*, 109−133.

(4) Li, J.; Lai, S. N.; Chen, D. A.; Wu, R. J.; Kobayashi, N.; Deng, L. S.; Huang, H. Y. A Review on Combustion Characteristics of Ammonia as a Carbon-Free Fuel. *Front. Energy Res.* **2021**, *9*, 760356.

(5) Valera-Medina, A.; Marsh, R.; Runyon, J.; Pugh, D.; Beasley, P.; Hughes, T.; Bowen, P. Ammonia−methane combustion in tangential swirl burners for gas turbine power generation. *Appl. Energy* **2017**, *185*, 1362−1371.

(6) Cesaro, Z.; Ives, M.; Nayak-Luke, R.; Mason, M.; Bañares-Alcántara, R. Ammonia to power: Forecasting the levelized cost of electricity from green ammonia in large-scale power plants. *Appl. Energy* **2021**, *282*, 116009.

(7) Rocha, R. C.; Ramos, C. F.; Costa, M.; Bai, X.-S. Combustion of NH3/CH4/Air and NH3/H2/Air Mixtures in a Porous Burner: Experiments and Kinetic Modeling. *Energy Fuels* **2019**, *33*, 12767−12780.

(8) Franco, M. C.; Rocha, R. C.; Costa, M.; Yehia, M. Characteristics of NH3/H2/air flames in a combustor fired by a swirl and bluff-body stabilized burner. *Proc. Combust. Inst.* **2021**, *38*, 5129−5138.

(9) Khateeb, A. A.; Guiberti, T. F.; Zhu, X.; Younes, M.; Jamal, A.; Roberts, W. L. Stability limits and NO emissions of technically-premixed ammonia-hydrogen-nitrogen-air swirl flames. *Int. J. Hydrogen Energy* **2020**, *45*, 22008−22018.

(10) Li, Z.; Li, S. Kinetics modeling of NOx emissions characteristics of a NH3/H2 fueled gas turbine combustor. *Int. J. Hydrogen Energy* **2021**, *46*, 4526−4537.

(11) Tang, G.; Jin, P.; Bao, Y.; Chai, W. S.; Zhou, L. Experimental investigation of premixed combustion limits of hydrogen and methane additives in ammonia. *Int. J. Hydrogen Energy* **2021**, *46*, 20765−20776.

(12) Wang, S.; Wang, Z.; Elbaz, A. M.; Han, X.; He, Y.; Costa, M.; Konnov, A. A.; Roberts, W. L. Experimental study and kinetic analysis of the laminar burning velocity of NH3/syngas/air, NH3/CO/air and NH3/H2/air premixed flames at elevated pressures. *Combust. Flame* **2020**, *221*, 270−287.

(13) Okafor, E. C.; Somarathne, K. D. K. A.; Ratthanan, R.; Hayakawa, A.; Kudo, T.; Kurata, O.; Iki, N.; Tsujimura, T.; Furutani, H.; Kobayashi, H. Control of NOx and other emissions in micro gas turbine combustors fuelled with mixtures of methane and ammonia. *Combust. Flame* **2020**, *211*, 406−416.

(14) Yang, Y.; Huang, Q.; Sun, J.; Ma, P.; Li, S. Reducing NOx Emission of Swirl-Stabilized Ammonia/Methane Tubular Flames through a Fuel-Oxidizer Mixing Strategy. *Energy Fuels* **2022**, *36*, 2277−2287.

(15) Zhang, M.; An, Z. H.; Wang, L.; Wei, X. T.; Jianayihan, B.; Wang, J. H.; Huang, Z. H.; Tan, H. Z. The regulation effect of methane and hydrogen on the emission characteristics of ammonia/

air combustion in a model combustor. *Int. J. Hydrogen Energy* **2021**, *46*, 21013−21025.
(16) Zhang, M.; Wei, X.; Wang, J.; Huang, Z.; Tan, H. The blow-off and transient characteristics of co-firing ammonia/methane fuels in a swirl combustor. *Proc. Combust. Inst.* **2021**, *38*, 5181−5190.
(17) He, Y.; Zheng, X.; Luo, J.; Zheng, H.; Zou, C.; Luo, G.; Zheng, C. Experimental and Numerical Study of the Effects of Steam Addition on NO Formation during Methane and Ammonia Oxy-Fuel Combustion. *Energy Fuels* **2017**, *31*, 10093−10100.
(18) Reiter, A. J.; Kong, S.-C. Combustion and emissions characteristics of compression-ignition engine using dual ammonia-diesel fuel. *Fuel* **2011**, *90*, 87−97.
(19) Okafor, E. C.; Naito, Y.; Colson, S.; Ichikawa, A.; Kudo, T.; Hayakawa, A.; Kobayashi, H. Measurement and modelling of the laminar burning velocity of methane-ammonia-air flames at high pressures using a reduced reaction mechanism. *Combust. Flame* **2019**, *204*, 162−175.
(20) Khateeb, A. A.; Guiberti, T. F.; Zhu, X.; Younes, M.; Jamal, A.; Roberts, W. L. Stability limits and exhaust NO performances of ammonia-methane-air swirl flames. *Exp. Therm Fluid Sci.* **2020**, *114*, 110058.
(21) Kurata, O.; Iki, N.; Matsunuma, T.; Inoue, T.; Tsujimura, T.; Furutani, H.; Kobayashi, H.; Hayakawa, A. Performances and emission characteristics of NH3−air and NH3CH4−air combustion gas-turbine power generations. *Proc. Combust. Inst.* **2017**, *36*, 3351−3359.
(22) Ju, Y.; Sun, W. Plasma assisted combustion: Dynamics and chemistry. *Prog. Energy Combust. Sci.* **2015**, *48*, 21−83.
(23) Starikovskiy, A.; Aleksandrov, N. Plasma-assisted ignition and combustion. *Prog. Energy Combust. Sci.* **2013**, *39*, 61−110.
(24) Shioyoke, A.; Hayashi, J.; Murai, R.; Nakatsuka, N.; Akamatsu, F. Numerical Investigation on Effects of Nonequilibrium Plasma on Laminar Burning Velocity of Ammonia Flame. *Energy Fuels* **2018**, *32*, 3824−3832.
(25) Faingold, G.; Lefkowitz, J. K. A numerical investigation of NH3/O2/He ignition limits in a non-thermal plasma. *Proc. Combust. Inst.* **2021**, *38*, 6661−6669.
(26) Choe, J.; Sun, W.; Ombrello, T.; Carter, C. Plasma assisted ammonia combustion: Simultaneous NOx reduction and flame enhancement. *Combust. Flame* **2021**, *228*, 430−432.
(27) Rajasegar, R.; Mitsingas, C. M.; Mayhew, E. K.; Yoo, J.; Lee, T. Proper Orthogonal Decomposition for Analysis of Plasma-Assisted Premixed Swirl-Stabilized Flame Dynamics. *IEEE Trans. Plasma Sci.* **2016**, *44*, 2940−2951.
(28) Ehn, A.; Petersson, P.; Zhu, J. J.; Li, Z. S.; Aldén, M.; Nilsson, E. J. K.; Larfeldt, J.; Larsson, A.; Hurtig, T.; Zettervall, N.; et al. Investigations of microwave stimulation of a turbulent low-swirl flame. *Proc. Combust. Inst.* **2017**, *36*, 4121−4128.
(29) Chintala, N.; Bao, A. N.; Lou, G. F.; Adamovich, I. V. Measurements of combustion efficiency in nonequilibrium RF plasma-ignited flows. *Combust. Flame* **2006**, *144*, 744−756.
(30) Pilla, G.; Galley, D.; Lacoste, D. A.; Lacas, F.; Veynante, D.; Laux, C. O. Stabilization of a turbulent premixed flame using a nanosecond repetitively pulsed plasma. *IEEE Trans. Plasma Sci.* **2006**, *34*, 2471−2477.
(31) Cui, W.; Ren, Y. H.; Li, S. Q. Stabilization of Premixed Swirl Flames Under Flow Pulsations Using Microsecond Pulsed Plasmas. *J. Propul. Power* **2019**, *35*, 190−200.
(32) Bak, M. S.; Do, H.; Mungal, M. G.; Cappelli, M. A. Plasma-assisted stabilization of laminar premixed methane/air flames around the lean flammability limit. *Combust. Flame* **2012**, *159*, 3128−3137.
(33) Lacoste, D. A.; Lee, B. J.; Satija, A.; Krishna, S.; Steinmetz, S. A.; Alkhesho, I.; Hazzaa, O.; Lucht, R. P.; Cha, M. S.; Roberts, W. L. Investigation of Gas Heating by Nanosecond Repetitively Pulsed Glow Discharges Used for Actuation of a Laminar Methane-Air Flame. *Combust. Sci. Technol.* **2017**, *189*, 2012−2022.
(34) Gao, J. L.; Kong, C. D.; Zhu, J. J.; Ehn, A.; Hurtig, T.; Tang, Y.; Chen, S.; Aldén, M.; Li, Z. S. Visualization of instantaneous structure and dynamics of large-scale turbulent flames stabilized by a gliding arc discharge. *Proc. Combust. Inst.* **2019**, *37*, 5629−5636.
(35) Lee, D. H.; Kim, K. T.; Cha, M. S.; Song, Y. H. Optimization scheme of a rotating gliding arc reactor for partial oxidation of methane. *Proc. Combust. Inst.* **2007**, *31*, 3343−3351.
(36) Ombrello, T.; Ju, Y.; Fridman, A. Kinetic Ignition Enhancement of Diffusion Flames by Nonequilibrium Magnetic Gliding Arc Plasma. *AIAA J.* **2008**, *46*, 2424−2433.
(37) Lin, B.; Wu, Y.; Zhu, Y.; Song, F.; Bian, D. Experimental investigation of gliding arc plasma fuel injector for ignition and extinction performance improvement. *Appl. Energy* **2019**, *235*, 1017−1026.
(38) Fridman, A.; Nester, S.; Kennedy, L. A.; Saveliev, A.; Mutaf-Yardimci, O. Gliding arc gas discharge. *Prog. Energy Combust. Sci.* **1999**, *25*, 211−231.
(39) Tang, Y.; Sun, J.; Shi, B.; Li, S.; Yao, Q. Extension of flammability and stability limits of swirling premixed flames by AC powered gliding arc discharges. *Combust. Flame* **2021**, *231*, 111483.
(40) Sun, J.; Tang, Y.; Li, S. Plasma-assisted stabilization of premixed swirl flames by gliding arc discharges. *Proc. Combust. Inst.* **2021**, *38*, 6733−6741.
(41) Tang, Y.; Xie, D.; Shi, B.; Wang, N.; Li, S. Flammability enhancement of swirling ammonia/air combustion using AC powered gliding arc discharges. *Fuel* **2022**, *313*, 122674.
(42) Lin, Q.; Jiang, Y.; Liu, C.; Chen, L.; Zhang, W.; Ding, J.; Li, J. Controllable NO emission and high flame performance of ammonia combustion assisted by non-equilibrium plasma. *Fuel* **2022**, *319*, 123818.
(43) Kee, R. J.; Miller, J. A.; Jefferson, T. H. *CHEMKIN: A General-Purpose, Problem-independent, Transportable, FORTRAN Chemical Kinetics Code Package*; Sandia Labs., 1980.
(44) Beer, J. M.; Chigier, N. A. *Combustion Aerodynamics*; Applied Science Publishers, 1974.
(45) Tang, Y.; Zhuo, J.; Cui, W.; Li, S.; Yao, Q. Non-premixed flame dynamics excited by flow fluctuations generated from Dielectric-Barrier-Discharge plasma. *Combust. Flame* **2019**, *204*, 58−67.
(46) d'Agostino, R.; Cramarossa, F.; De Benedictis, S.; Ferraro, G. Kinetic and spectroscopic analysis of NH3 decomposition under RF Plasma at moderate pressures. *Plasma Chem. Plasma Process.* **1981**, *1*, 19−35.
(47) Pugh, D.; Runyon, J.; Bowen, P.; Giles, A.; Valera-Medina, A.; Marsh, R.; Goktepe, B.; Hewlett, S. An investigation of ammonia primary flame combustor concepts for emissions reduction with OH*, NH2* and NH* chemiluminescence at elevated conditions. *Proc. Combust. Inst.* **2021**, *38*, 6451−6459.
(48) Pearse, R. W. B.; Gaydon, A. G.; Pearse, R. W. B.; Gaydon, A. G. *The Identification of Molecular Spectra*; Chapman and Hall London, 1976.
(49) Pu, G.; Huang, B.; Zhang, X.; Du, J.; Zhu, T.; Chen, B. Investigation of flame structure and burning intensity of partially premixed methane enrichment of syngas using OH-PLIF and kinetic simulation. *Combust. Theory Modell.* **2018**, *22*, 432−445.
(50) Kasim, M. F.; Holloway, J.; Ceurvorst, L.; Levy, M. C.; Ratan, N.; Sadler, J.; Bingham, R.; Burrows, P. N.; Trines, R.; Wing, M.; et al. Quantitative single shot and spatially resolved plasma wakefield diagnostics. *Phys. Rev. Spec. Top.–Accel. Beams* **2015**, *18*, 081302.
(51) Glarborg, P.; Miller, J. A.; Ruscic, B.; Klippenstein, S. J. Modeling nitrogen chemistry in combustion. *Prog. Energy Combust. Sci.* **2018**, *67*, 31−68.
(52) Rutar, T.; Malte, P. C. NOx Formation in High-Pressure Jet-Stirred Reactors With Significance to Lean-Premixed Combustion Turbines. *J. Eng. Gas Turbines Power* **2002**, *124*, 776−783.
(53) Turányi, T. Sensitivity analysis of complex kinetic systems. Tools and applications. *J. Math. Chem.* **1990**, *5*, 203−248.

https://doi.org/10.1021/acs.energyfuels.2c01217
Energy Fuels 2022, 36, 8520−8527